Desalination and Water Treatment
www.deswater.com

doi: 10.5004/dwt.2019.24051

155 (2019) 197–206
July

Phenol adsorption onto kaolin and fuller's earth: a comparative study with bentonite

Safwat M. Safwat[a,*], Mohamed Medhat[b], Hisham Abdel-Halim[a]

[a]*Sanitary & Environmental Engineering Division, Faculty of Engineering, Cairo University, PO Box 12613, Giza, Egypt, Tel. +201092525159; Fax: +20235689210; emails: safwat@ualberta.ca (S.M. Safwat), hishama.halim2011@gmail.com (H. Abdel-Halim)*
[b]*Sanitary & Environmental Engineering Division, EnviroConsult, Cairo, Egypt, email: mmedhat93@hotmail.com*

Received 31 October 2018; Accepted 1 March 2019

ABSTRACT

The uptake of phenol using kaolin and fuller's earth and the comparison of their effects with bentonite are investigated in this study. In addition, X-ray fluorescent, X-ray diffraction, and thermogravimetric analyzes were carried out to examine the characteristics of the three adsorbents. Adsorption of phenol as a function of pH level was also investigated. The points of zero charge for kaolin, fuller's earth, and bentonite were determined to be 5.9, 8, and 7.7, respectively. To study the adsorption kinetics and mechanisms, various kinetic models were explored. Two-parameter and three-parameter isotherm models were employed for equilibrium studies. The results showed that decreasing the pH value led to an increase in phenol uptake. The maximum removal efficiencies were 34.35%, 23%, and 42.63% for kaolin, fuller's earth, and bentonite, respectively, for 0.5 g of adsorbent and pH = 4.5. Phenol uptake on the three adsorbents can be expressed by pseudo-second order kinetics. Whereas the Freundlich isotherm suits the experimental data for adsorption onto bentonite and fuller's earth, the Temkin isotherm well suits the experimental data for uptake onto kaolin. The Fourier transform infrared and scanning electron microscope were used in the analysis of the adsorbents surface prior to and after the process of adsorption.

Keywords: Clay; Isotherms; Kinetics; Montmorillonite; Palygorskite; Pyrophyllite

1. Introduction

Phenol is an organic compound that can be found in industrial wastewaters [1]. Since it is toxic and has the ability to accumulate in the environment, it is a high-priority concern [2]. When the concentration of phenol reaches between 10 and 24 mg l^{-1}, it can be toxic for humans [3]. Oil refineries, synthetic rubber, petrochemical, coal conversion, and other industries are among the main sources of high concentrations of phenolic compounds [1]. Thus, effluent from these sources can reach water courses and wastewater treatment plants. Phenol can cause several problems, as it is toxic to aquatic species and can inhibit the biological treatment processes in treatment plants [4,5]. Numerous technologies have been investigated to eliminate phenol from wastewater, such as chemical oxidation, osmosis, ion exchange, electrochemical methods, membrane filtration, microbial fuel cells, precipitation, and coagulation [2,6,7]. However, these technologies have some issues, such as high cost, low efficiency, and toxic by-products [1,8].

The adsorption process is considered a suitable technology for wastewater treatment due to its simplicity, ease of operation, excellent performance, and safety for the environment [9,10]. In the adsorption process, the pollutant is transferred from a liquid phase and is accumulated into a solid phase [11]. The most widely used adsorbent is activated carbon. It is efficient in removing various types of pollutants, such as heavy metals and toxic pollutants

* Corresponding author.

[9]. However, research has been focused on investigating other types of adsorbents due to the high cost, as activated carbon is formed from an expensive raw material [12]. Low cost adsorbents can be waste products, such as fly ash and sludges, or natural materials, such as clay, red mud, and chitosan [13]. Adsorbents from raw clay, such as kaolin, fuller's earth, and bentonite, have many advantages. They are low cost, abundant, and non-toxic to the environment and have excellent adsorption properties and a high specific surface area [14]. Kaolin, fuller's earth, and bentonite have shown excellent performance in adsorption of various pollutants, such as heavy metals, methylene blue, mercury, dyes, and other contaminants [15–19].

Phenol uptake through adsorption has been investigated using activated carbon, functional chitosan, silica gel, activated alumina, and other adsorbents [20–24]. The processing cost of large-scale phenol removal will increase when using carbonaceous adsorbents or modified natural minerals [25]. As a result, it is essential to examine the ability of phenol uptake using unmodified natural adsorbents as an alternative to high-cost technology [24]. To the best of our knowledge, no report has been presented on the adsorption of phenol from effluents using kaolin and fuller's earth. Thus, this study was performed to examine the ability of both kaolin and fuller's earth to remove phenol from wastewater via adsorption and to compare the performance of each with bentonite. The exploration of the experimental data from the adsorption procedure was conducted by fitting the data to the pseudo-first order (PFO) and pseudo-second order (PSO), with Elovichs' equation, the intra-particle diffusion model, and the Boyd kinetic model in determining the kinetics and mechanisms of adsorption. After that, suitable isotherms to express the adsorption of phenol onto the three adsorbents were determined by fitting the equilibrium data to various two-parameter and three-parameter isotherm models.

2. Materials and methods

2.1. Properties of wastewater and natural adsorbents

A certain amount of phenol (LobaChemie, India) was dissolved into distilled water to prepare synthetic wastewater with the required concentration. Three adsorbents were examined: kaolin (*K*), fuller's earth (*F*), and bentonite (*B*) (LobaChemie, India). The values of the specific surface area for kaolin, fuller's earth, and bentonite were 53, 40, and 63 $m^2\ g^{-1}$, respectively. The element constituents in the three adsorbents were determined using X-ray fluorescence (XRF) spectrometry as shown in Table 1. The analysis showed that silicon dioxide is the predominant constituent in kaolin, fuller's earth, and bentonite, and the percentages are 63.68%, 52.32%, and 50.32%, respectively. The second predominant constituent is aluminum oxide in kaolin (29.26%), magnesium oxide in fuller's earth (10.30%), and aluminum oxide in bentonite (20.64%). The three adsorbents were investigated through X-ray diffraction (XRD) patterns using X'Pert PRO with Monochromator with Cu-radiation as shown in Figs. 1(a)–(c). Parameter calculations were performed at 45 kV and 35 mA, and the peaks of reflection were obtained using a 0.03° sec^{-1} scanning rate at 2 θ between 2° and 60°. From the XRD spectra, it was demonstrated that there are regular crystalline planes to reflect X-rays. The XRD spectra revealed that the three adsorbents consist of natural clay minerals besides a few impurities. Kaolin, fuller's earth, and bentonite show several reflection peaks, and the presence of pyrophyllite, palygorskite, and montmorillonite, respectively. These minerals are consistent with XRF analysis. Since peaks are present, the three adsorbents are of crystalline nature. Thermogravimetric analysis (TGA) was used to investigate the thermal stability of the three adsorbents as shown in Fig. 1(d). The TGA thermal analyzer (TGA-50H) was operated with a heating rate of 20°C min^{-1}, and a flow rate of nitrogen atmosphere of 20 mL min^{-1}. For kaolin, there is a smooth small mass loss. The mass loss at 700°C was around 2.65%. For fuller's earth and bentonite, there are two main mass loss steps: the initial step occurred at temperatures up to 160°C, and the second step occurred at the temperature range of 160°C–700°C. The initial step corresponded to a mass loss of up to 10.5%. This mass loss is credited to the desorption of the adsorbed water [26]. On the other hand, the second step corresponded to a mass loss of up to 19.5% for fuller's earth, and of up to 16.5% for bentonite. This mass loss is credited to the decomposition of fuller's earth and bentonite [10,27]. Comparing the degradation of kaolin to the thermal degradation of fuller's earth and bentonite, fuller's earth and bentonite have faster mass loss. The pH drift method was used to determine the point of zero charge according to procedures explained elsewhere [28,29]. The points of zero charge (pH_{pzc}) for kaolin, fuller's earth, and bentonite were 5.9, 8, and 7.7, respectively, as shown in Fig. 1(e).

2.2. Experiment setup and operating procedures

Adsorption experiments were performed using the batch experimental approach at 20°C ± 2°C. At three dissimilar pH values (4.5, 7.0, and 9.5), a certain mass of either adsorbent was shaken with 30 ml of aqueous solution of phenol in flasks at 100 rpm. Either 0.1 N of diluted hydrochloric acid (HCl) or 0.1 N of diluted sodium hydroxide (NaOH) was used to adjust the pH. For each withdrawn sample, a 0.45-micron filter paper (Whatman no. 1) was used to filter it. All the kinetic experiments were performed at an optimum pH. Equilibrium studies were performed by adding various adsorbent doses (0.5–5 g) to a 30 ml solution of phenol of known concentration. After that, samples were shaken to determine the equilibrium condition. Quantitative determination of phenol was done using the digital photometer NANOCOLOR® 500 D (MACHEREY-NAGEL). The photometric determination method was used with diazotized 4-nitroaniline at a wavelength of 470 nm. Control experiments, with no added adsorbents, were performed side by side with adsorption experiments to verify phenol stability during the experiments. To determine the change in fingerprint before and after adsorption for the three adsorbents, Fourier transform infrared (FTIR) spectroscopy was conducted. A scanning electron microscope (SEM) was used to examine the morphology of the three adsorbents before and after the phenol uptake.

Table 1
Elemental constituents of kaolin, fuller's earth, and bentonite

Elements	SiO_2	TiO_2	Al_2O_3	Fe_2O_3	MnO	MgO	CaO	Na_2O	K_2O	P_2O_5	Cl	SO_3	L.O.I
% in Kaolin	63.68	0.34	29.26	0.33	0.01	0.08	0.02	0.01	1.06	0.02	<0.01	<0.01	4.84
% in Fuller's earth	52.32	1.27	6.77	8.82	0.17	10.30	4.47	0.06	0.66	0.06	<0.01	<0.01	14.99
% in Bentonite	50.32	1.92	20.64	9.94	0.10	2.37	0.73	3.19	0.99	0.11	2.24	0.31	6.99

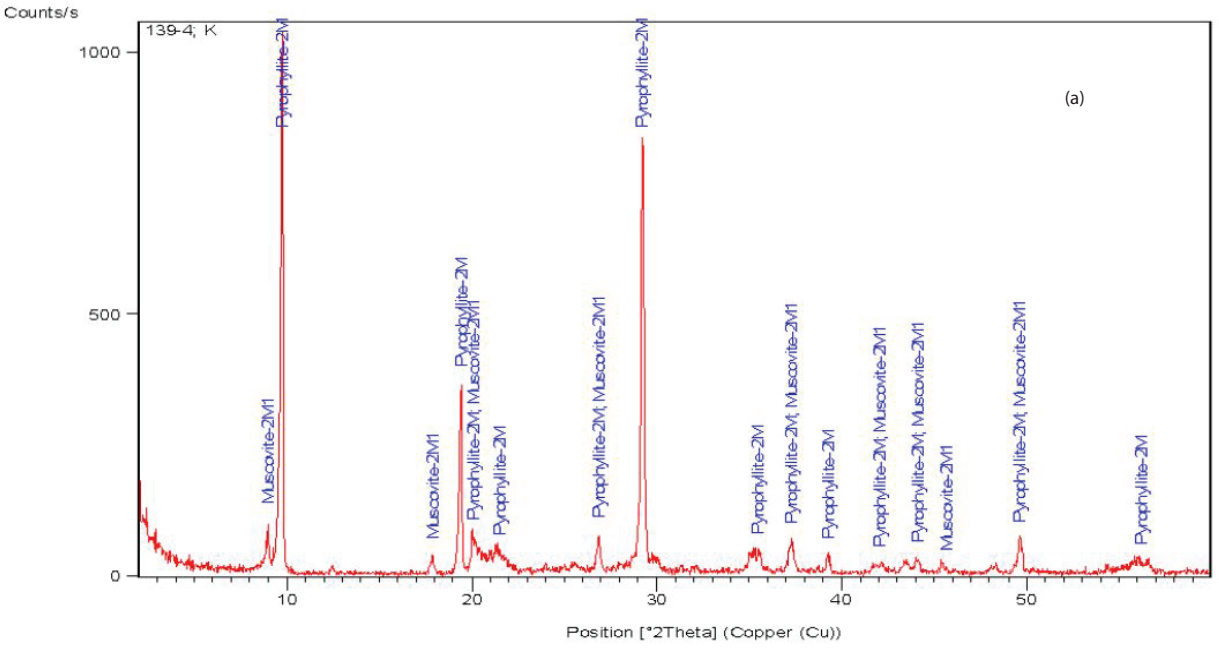

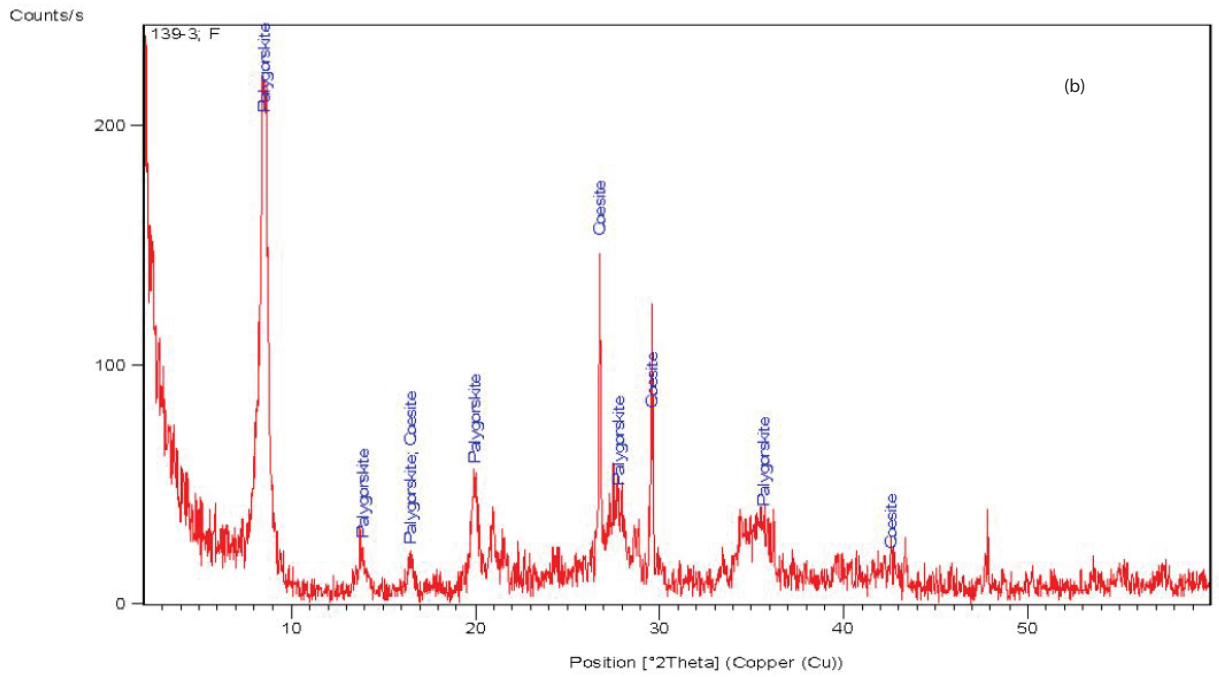

Fig. 1. *(Continued)*)

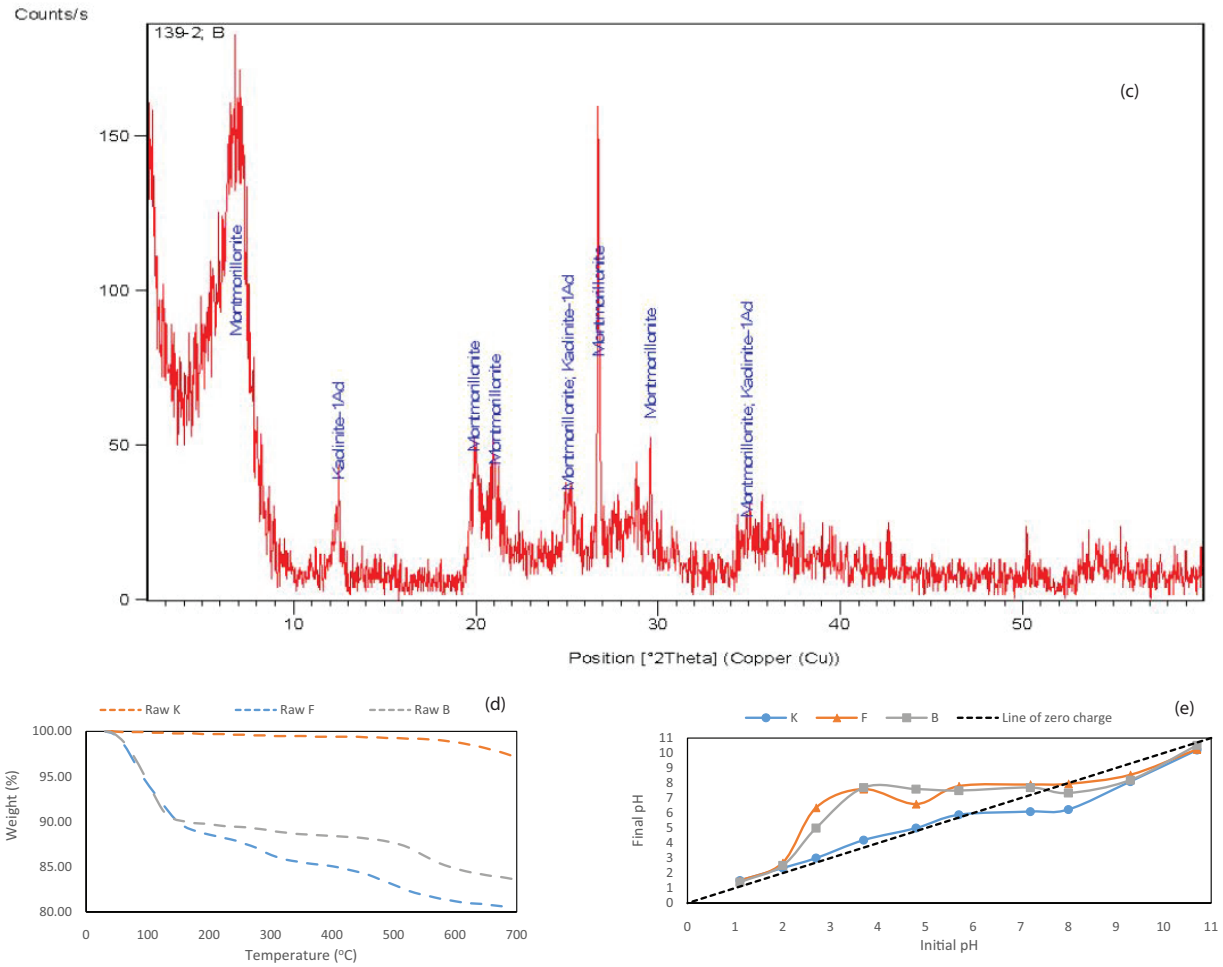

Fig. 1. (a) Scanning XRD spectrum of kaolin, (b) scanning XRD spectrum of fuller's earth, (c) scanning XRD spectrum of bentonite, (d) TGA of three adsorbents, and (e) pH drift method.

3. Results and discussion

3.1. Effect of initial pH on phenol removal

The initial pH value influences adsorption. To achieve the optimum pH for phenol adsorption for all three adsorbents, the removal of phenol as a function of pH was analyzed. Fig. 2 shows that the efficiency of phenol removal dropped with the rising pH value. The maximum removal efficiencies were 34.35%, 23% and 42.63% for kaolin, fuller's earth, and bentonite, respectively, for an adsorbent mass of 0.5 g at pH = 4.5 at an initial concentration of phenol of 150 mg l^{-1}.

Owing to its capacity to behave like a weak acid, phenol will dissociate, as illustrated in Eq. (1). The surface of the adsorbent will be charged positively until pH < pH_{pzc} [30,31]. The surface of the adsorbent in alkaline solution will be charged negatively, while a shift of the equilibrium equation will take place to the right. For that reason, a decline in the adsorption will occur since repulsion forces of comparable charges exist [19]. The surface of the adsorbent will be charged positively in an acidic solution [31]. Because there will be a shift to the left for the equilibrium equation in acidic solution, the phenol adsorption will take place through dipole-dipole interaction, whereby the negatively charged phenol hydroxyl group will interact with the positively charged functional group on the surface of the adsorbent [10]. Therefore, the phenol adsorption would have a higher stronger interaction with the adsorbents, and thus, a higher uptake at low pH values.

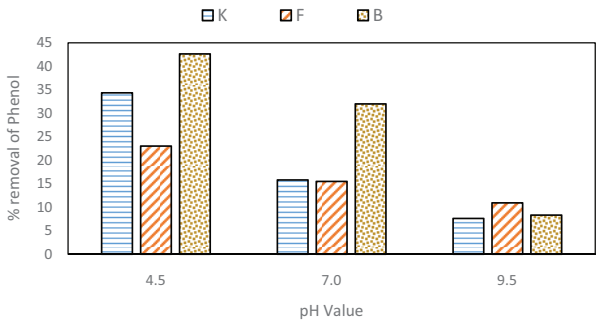

Fig. 2. Removal efficiency of phenol at different pH values using kaolin, fuller's earth, and bentonite.

$$C_6H_5OH_{(aq)} + H_2O_{(l)} \rightarrow C_6H_5O^-_{(aq)} + H_3O^+_{(aq)} \quad (1)$$

3.2. Kinetics studies

After pre-set time intervals of 5 min for a period of 24 h, flasks were progressively withdrawn from the shaker for the kinetic experiments. Then, the concentration of phenol was determined for each sample after filtration [32]. A mass balance relationship was used to determine q_t (mg g^{-1}), which is the amount of phenol adsorbed onto the adsorbents at each time, as shown in Eq. (2):

$$q_t = (C_0 - C_t) \times (V/W) \tag{2}$$

where the initial liquid-phase phenol concentration is represented by C_0 (mg l^{-1}), the liquid-phase phenol concentration at time t (min) is represented by C_t (mg l^{-1}), the solution volume (l) is represented by V, and the adsorbent mass (g) is represented by W. Various models were assessed to investigate phenol adsorption kinetics. These models were the PFO, PSO, and Elovich's equation [33–35]. The three models can be expressed as shown in the following equations (Eqs. (4–6)):

$$q_t = q_e\left(1 - e^{-k_1 t}\right) \tag{3}$$

$$q_t = \frac{q_e^2 k_2 t}{1 + q_e k_2 t} \tag{4}$$

$$q_t = \frac{1}{\beta}\ln\left(1 + \alpha\beta t\right) \tag{5}$$

where the PFO and PSO rate constants are represented by k_1 (min^{-1}) and k_2 (mg g^{-1}.min) respectively, the amount of phenol adsorbed at equilibrium is represented by q_e, the initial rate constant is represented by α (mg g^{-1}.min), and the desorption constant for any single experiment is represented by β (mg g^{-1}). [10]. To make the aforementioned equations linear, $\ln(q_e - q_t)$ against time was plotted for the PFO expression, t/q_t against time was plotted for the PSO expression, and q_t against ln$t$ was plotted for Elovich's equation as illustrated in Figs. 3(a)–(c). In all cases, the calculations of the resultant correlation coefficients (R^2) were calculated. The results of the experiment best suit the PSO for kaolin (R^2 = 0.9844), fuller's earth (R^2 = 0.9933), and bentonite (R^2 = 0.9982). This implies that the adsorption of phenol onto the three natural adsorbents is capable of being properly estimated by the PSO kinetic model. Furthermore, K_2 and q_e were found to be 0.0627 g mg^{-1}.min and 0.434 mg g^{-1} for kaolin, respectively, 0.129 g mg^{-1}.min and 0.3227 mg g^{-1} for fuller's earth, respectively, and 0.1306 g mg^{-1}.min and 0.5446 mg g^{-1} for bentonite, respectively.

3.3. Adsorption mechanisms

In the adsorption process, it is not possible for the aforementioned kinetic models to depict the diffusion mechanism and rate-controlling steps [36]. It is important to note that the three consecutive steps can occur during the adsorption process as follows [37]:

(i) Film diffusion whereby the phenol moves from the bulk solution to the clay's outer surface,
(ii) Particle diffusion whereby the phenol migrates via the interior of the clay particles,
(iii) Phenol uptake on the clay's interior surface.

An intra-particle diffusion model was explored to demonstrate the adsorption mechanism [38]. The following equation (Eq. (6)) can be used to determine the intra-particle diffusion model:

$$q_t = K_p\sqrt{t} + C \tag{6}$$

where the intra-particle diffusion model rate constant is represented by k_p (mg g^{-1}. min$^{0.5}$) and the constant associated with the boundary layer thickness is represented by C (mg g^{-1}) [39]. Fig. 3(d) displays the plot of phenol uptake against $t^{1/2}$ for the three adsorbents. It is possible to divide the plots for phenol uptake onto the three adsorbents into two linear portions. This is a sign of a multistep mechanism influencing the adsorption process [39]. The surface adsorption or rapid external diffusion stage is the first part, while the gradual adsorption stage, which the intra-particle diffusion controls, is the second linear part [40]. The value K_p was calculated and found to be 0.0068 mg g^{-1}.min$^{0.5}$ for kaolin, 0.005 mg g^{-1}.min$^{0.5}$ for fuller's earth, and 0.0074 mg g^{-1}.min$^{0.5}$ for bentonite.

Differentiating film diffusion from particle diffusion of adsorbate molecules is very essential. Boyd kinetic model was used to identify the slowest step in the adsorption process. The following equation expresses the Boyd kinetic equation [41]:

$$\frac{q_t}{q_e} = 1 - \frac{6}{\pi^2}\exp\left(-Bt\right) \tag{7}$$

where the mathematical function q_t/q_e is represented by Bt. [10]. The value of Bt was determined at various contact times and was plotted versus time t as illustrated in Fig. 3(e). As the plots are linear but do not pass through the origin for the three adsorbents, the adsorption of phenol is influenced by film diffusion [10].

3.4. Equilibrium studies

To attain equilibrium, based on the kinetic results, the flasks were shaken for 24 h. The equilibrium phenol concentration was determined for each sample after filtration (C_e, mg l^{-1}). The following mass balance relationship was used to determine q_e (mg g^{-1}), which is the quantity of phenol adsorbed onto the adsorbents at the equilibrium as shown in Eq. (8):

$$q_e = (C_0 - C_e) \times (V/W) \tag{8}$$

Five various isotherms were tested using the adsorption equilibrium results. These isotherms were the Freundlich isotherm [42], Langmuir isotherm [43], Temkin isotherm [44], Dubinin-Radushkevich isotherm [45], and Redlich-Peterson

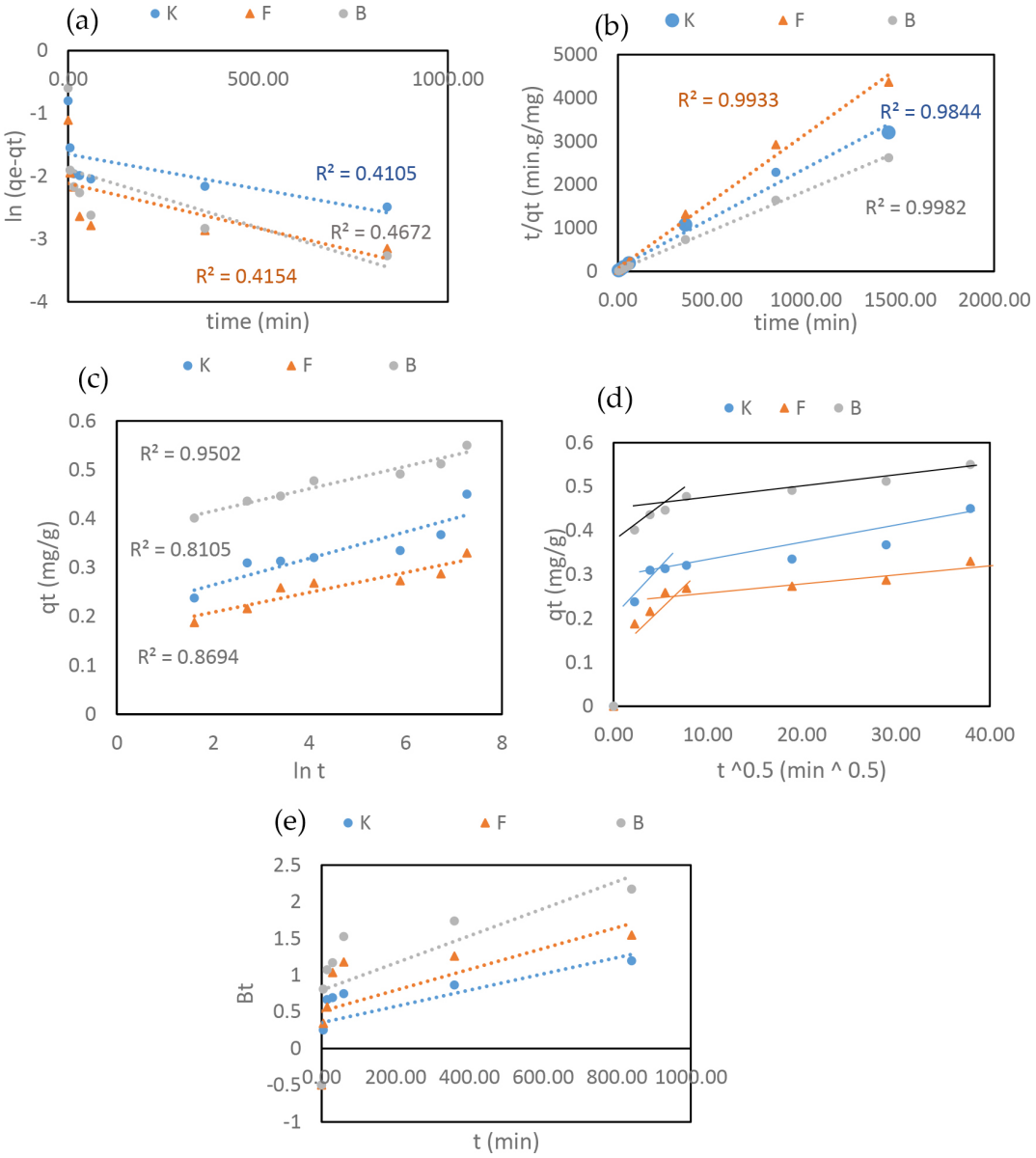

Fig. 3. Kinetics (a) pseudo first-order, (b) pseudo second-order, (c) Elovich, (d) intra-particle diffusion model, and (e) Boyd kinetic model.

isotherm [46]. The following equations (Eqs. (9–13)) demonstrate the mathematical expression for each isotherm:

$$q_e = K_F C_e^n \tag{9}$$

$$q_e = \frac{q_m K_L C_e}{1 + K_L C_e} \tag{10}$$

$$q_e = B_1 \ln(K_T C_e) \tag{11}$$

$$q_e = q_m \exp(-Be^2) \tag{12}$$

$$q_e = \frac{K_{RP} C_e}{1 + a_{RP} C_e^g} \tag{13}$$

where the Freundlich adsorption constant (mg g^{-1} (mg l^{-1})^n) is represented by K_F, the non-linearity degree is represented by n, the maximum adsorption capacity (mg g^{-1}) is represented by q_m, the Langmuir coefficient is represented by K_L (l mg^{-1}); $B_1 = RT/b$, the absolute temperature in K is represented by T, the universal gas constant (8.314 J mol.K^{-1}) is represented by R, the equilibrium binding constant (l mg^{-1}) is represented by K_T, the Redlich-Peterson constants are represented by K_{RP} (l g^{-1}) and a_{RP} (mg L^{-1})$^{-g}$, an exponent with a value between 0 and 1 is represented by g (dimensionless), and e is the Polanyi potential. Table 2 shows the values of R^2 corresponding to various equilibrium isotherms. Table 3 shows the results

of the three natural adsorbents for the Redlich-Peterson isotherm. The Temkin isotherm (R^2 = 0.9803) better fits the results of kaolin, and its equation is shown in Eq. (14). Besides, K_T was found to be 13.75 × 10^{-3} l mg^{-1}, and B_1 was 9.821 mg l^{-1}. The fuller's earth data matched the Freundlich isotherm (R^2 = 0.9622), and its equation is shown in Eq. (15). Furthermore, n was found to be 9.538, and K_F was 4.168 × 10^{-20} (mg g^{-1})/(mg l^{-1})$^{9.538}$. The results of bentonite closely matched the Freundlich isotherm (R^2 = 0.9752), and its equation is shown in Eq. (16). Likewise, n was found to be 5.022, and K_F was 7.12 × 10^{-10} (mg g^{-1})/(mg l^{-1})$^{5.022}$. There are certain assumptions about the adsorption occurrence that each isotherm possesses. The Temkin isotherm assumes that the adsorption heat decreases linearly with the surface coverage. In the Freundlich adsorption isotherm, adsorption occurrence onto a heterogeneous surface happens via several layers of adsorption mechanisms. Figs. 4(a)–(c) show the equilibrium and the calculated data of the best model. For comparison, the phenol adsorption capacities of reported adsorbents were given in Table 4. The values of adsorption capacity obtained from this study were different than the values obtained from previous studies. This may be due to the difference in (1) the phenol initial concentration and (2) the values of the specific surface area.

$$q_e = 9.821 \ln C_e - 42.099 \quad (14)$$

$$\log q_e = 9.538 \log C_e - 19.38 \quad (15)$$

$$\log q_e = 5.022 \log C_e - 9.1475 \quad (16)$$

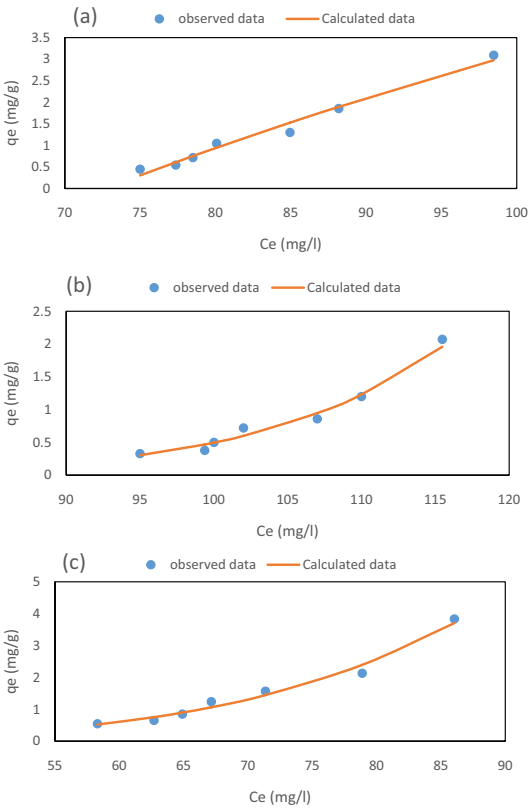

Fig. 4. Observed and calculated equilibrium data by the best model (a) kaolin, (b) fuller's earth, and (c) bentonite.

3.5. FTIR spectroscopy

The FTIR was applied in examining the alterations in the fingerprints for kaolin, fuller's earth, and bentonite due to phenol adsorption as shown in Figs. 5(a)–(c), respectively. The FTIR spectra demonstrated a band between 800 and 1,200 cm^{-1} for the three natural adsorbents, ascribing to the Si–O stretching band [19]. The finger print region, ranging from 400 to 1,500 cm^{-1}, exhibits variations among the spectra

Table 2
Values of R^2 corresponding to various equilibrium isotherms

	Freundlich	Langmuir	Temkin	Dubinin-Radushkevich
Kaolin	0.9488	0.8223	0.9803	0.9699
Fuller's earth	0.9622	0.9085	0.89	0.9532
Bentonite	0.9752	0.9207	0.9064	0.9635

Table 4
Comparison of phenol adsorption on reported adsorbents

Adsorbent	Adsorption capacity (mg g^{-1})	Reference
Granular activated carbon	75.5	[47]
Aluminum oxide	0.35	[48]
Zinc oxide	0.28	[48]
Titanium dioxide	0.44	[48]
Dried azolla	24.6	[49]
Petroleum coke	6.0	[50]
Rice husk	4.5	[50]
Natural coal	18.8	[51]
Red mud	4.13	[52]
Kaolin	0.3	This study
Fuller's earth	0.31	This study
Bentonite	0.52	This study

Table 3
Redlich-Peterson isotherm of phenol onto kaolin, fuller's earth, and bentonite

Adsorbent	g	0.01	0.1	0.2	0.3	0.4	0.5	0.6	0.7	0.8	0.9	1
Kaolin	R^2	0.7956	0.7931	0.7902	0.7873	0.7844	0.7815	0.7786	0.7757	0.7727	0.7698	0.7668
Fuller's earth	R^2	0.8973	0.8965	0.8956	0.8946	0.8937	0.8928	0.8918	0.8908	0.8898	0.8888	0.8878
Bentonite	R^2	0.402	0.4061	0.4106	0.4152	0.4198	0.4244	0.429	0.4336	0.4382	0.4428	0.4475

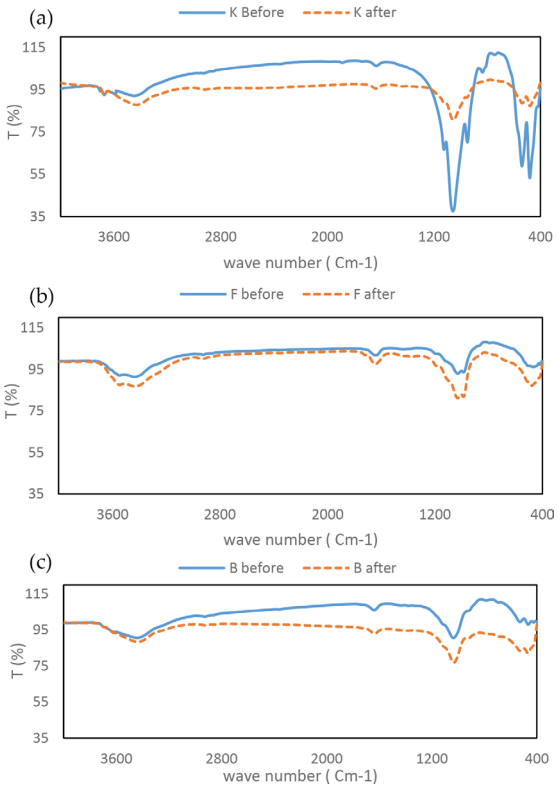

Fig. 5. FTIR spectra of (a) kaolin, (b) fuller's earth, and (c) bentonite.

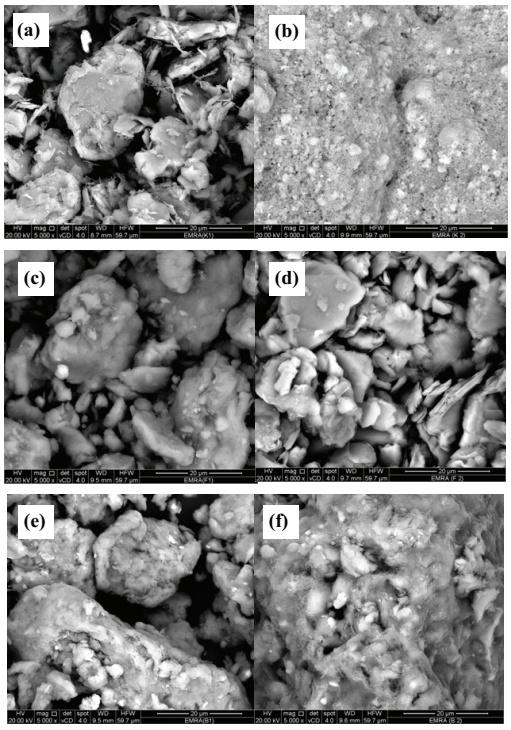

Fig. 6. SEM images (a) kaolin before phenol uptake, (b) kaolin after phenol uptake, (c) fuller's earth before phenol uptake, (d) fuller's earth after phenol uptake, (e) bentonite before phenol uptake, and (f) bentonite after phenol uptake.

of the three adsorbents before and following the adsorption occurrence. This difference is owed to the adsorption phenomena. Such a difference is substantiated using the manifestation of peaks between 3,000 and 3,600 cm^{-1} in the three adsorbents' spectra following the adsorption event, signifying the existence of the O–H group as a result of phenol adsorption.

3.6. Morphologies of kaolin, fuller's earth, and bentonite

Current research illustrates that surface morphology, along with chemical composition, have a considerable effect on adsorption capacity [25]. The SEM images of kaolin, fuller's earth, and bentonite prior to and following phenol adsorption are displayed in Fig. 6. The SEM images for the three adsorbents display rough and irregular surfaces with porous openings prior to adsorption. Apart from fuller's earth, the porous openings disappeared at the end of experiments. This indicates the low removal efficiency of phenol using fuller's earth compared with both kaolin and bentonite. A pronounced change in the morphologies is revealed by the SEM images, confirming adsorption.

4. Conclusion

Three dissimilar adsorbents (kaolin, fuller's earth, and bentonite) were used to examine adsorption of phenol. The results revealed the dependence of adsorption on pH, and the increased phenol removal efficiency with a decreasing pH value. The PSO kinetics can be used to express the uptake of phenol onto the three adsorbents. The adsorption mechanism of phenol was controlled using a multistep mechanism as indicated by the intra-particle adsorption model. There is an indication via the Boyd kinetic model of the possibility of liquid-film diffusion involvement in the control of the phenol adsorption on the three adsorbents. Phenol uptake at equilibrium could be expressed by the Temkin isotherm for kaolin, and the Freundlich isotherm for both fuller's earth and bentonite. The results of the FTIR spectroscopy displayed changes in the fingerprint for the three adsorbents before and after the phenol uptake. The SEM images displayed porous openings in the three adsorbents before adsorption. The adsorption occurrence was confirmed by the change in adsorbent morphologies.

Acknowledgment

The authors wish to thank the specialists at Micro Analytical Center, Cairo University; and the central laboratory of Egyptian mineral resources authority for help with the analyses. This research did not receive any specific grant from funding agencies in the public, commercial, or not-for-profit sectors.

Symbols

a_{RP} – Redlich-Peterson constant, $(mg\ l^{-1})^{-g}$
C – Constant associated with the boundary layer thickness, $mg\ g^{-1}$
C_0 – Initial liquid-phase phenol concentration, $mg\ l^{-1}$
C_e – Equilibrium phenol concentration, $mg\ l^{-1}$

C_t – Liquid-phase phenol concentration at time t, min mg l^{-1}
E – Polanyi potential
G – An exponent with a value ranging between 0 and 1
K – Absolute temperature, K
k_1 – PFO rate constant, min^{-1}
k_2 – PSO rate constant, mg g^{-1}.min
K_F – Freundlich adsorption constant, mg g^{-1} (mg $l^{-1})^n$
K_L – Langmuir coefficient, l mg^{-1}
k_p – Intra-particle diffusion model rate constant, mg g^{-1}. $min^{0.5}$
K_{RP} – Redlich-Peterson constant, l g^{-1}
K_T – Equilibrium binding constant, l mg^{-1}
n – Non-linearity degree in Freundlich adsorption isotherm
q_e – Amount of phenol adsorbed at equilibrium, mg g^{-1}
q_m – Maximum adsorption capacity, mg g^{-1}
V – Solution volume, l
W – Adsorbent mass, g
α – Initial rate constant, mg g^{-1}.min
β – Desorption constant for any single experiment, mg g^{-1}

References

[1] M.A. Zazouli, M. Taghavi, Phenol removal from aqueous solutions by electrocoagulation technology using iron electrodes:effect of some variables, J. Water Resour. Prot., 4 (2012) 980–983.
[2] S.H. Lin, R.S. Juang, Adsorption of phenol and its derivatives from water using synthetic resins and low-cost natural adsorbents: a review, J. Environ. Manage., 90 (2009) 1336–1349.
[3] J.P. Kulkarni, J Sunil Kaware, Review on research for removal of phenol from wastewater, Int. J. Sci. Res. Publ., 3 (2013) 1–5.
[4] S.M. Borghei, S.H. Hosseini, The treatment of phenolic wastewater using a moving bed biofilm reactor, Process Biochem., 39 (2004) 1177–1181.
[5] S.M. Safwat, Performance of Moving Bed Biofilm Reactor Using Effective Microorganisms, J. Cleaner. Prod., 185 (2018) 723–731.
[6] E. Bazrafshan, H. Biglari, A.H. Mahvi, Phenol removal by electrocoagulation process from aqueous solutions, Fresenius Environ. Bull., 21 (2012) 364–371.
[7] S. Ahmed, E. Rozaik, H. Abdelhalim, Effect of Configurations, Bacterial adhesion, and anode surface area on performance of microbial fuel cells used for treatment of synthetic wastewater, Water Air Soil Pollut., 226 (2015) 300.
[8] S.M. Safwat, A. Hamed, E. Rozaik, Electrocoagulation/electroflotation of real printing wastewater using copper electrodes: a comparative study with aluminum electrodes, Sep. Sci. Technol, 54 (2019) 183–194. doi:10.1080/01496395.2018.1494744.
[9] S. De Gisi, G. Lofrano, M. Grassi, M. Notarnicola, Characteristics and adsorption capacities of low-cost sorbents for wastewater treatment: a review, Sustainable Mater. Technol., 9 (2016) 10–40.
[10] S. Safwat, M. Matta, Adsorption of urea onto granular activated alumina: a comparative study with granular activated carbon, J. Dispers. Sci. Technol., 39 (2018) 1699–1709.
[11] J.C. Crittenden, R.R. Trussell, D.W. Hand, K.J. Howe, G. Tchobanoglous, Introduction to adsorption phenomena, Adsorpt. MWH's Water Treat Princ. Des. (2012). doi:10.1002/9781118131473.ch15.
[12] S.P.D. Kaman, I.A.W. Tan, L.L.P. Lim, Palm oil mill effluent treatment using coconut shell – based activated carbon: adsorption equilibrium and isotherm, MATEC Web Conf., 87 (2017) 03009. doi:10.1051/matecconf/20178703009.
[13] M. Ahmaruzzaman, Adsorption of phenolic compounds on low-cost adsorbents: a review, Adv. Colloid Interface Sci., 143 (2008) 48–67.
[14] M.K. Uddin, A review on the adsorption of heavy metals by clay minerals, with special focus on the past decade, Chem. Eng. J., 308 (2017) 438–462.
[15] T.S. Anirudhan, M. Ramachandran, Adsorptive removal of basic dyes from aqueous solutions by surfactant modified bentonite clay (organoclay): kinetic and competitive adsorption isotherm, Process Saf. Environ. Prot., 95 (2015) 215–225.
[16] A.K. Bhattacharya, T.K. Naiya, S.N. Mandal, S.K. Das, Adsorption, kinetics and equilibrium studies on removal of Cr(VI) from aqueous solutions using different low-cost adsorbents, Chem. Eng. J., 137 (2008) 529–541.
[17] J.U.K. Oubagaranadin, N. Sathyamurthy, Z.V.P. Murthy, Evaluation of Fuller's earth for the adsorption of mercury from aqueous solutions: a comparative study with activated carbon, J. Hazard. Mater., 142 (2007) 165–174.
[18] Y. Bulut, H. Karaer, Adsorption of methylene blue from aqueous solution by crosslinked chitosan/bentonite composite, J. Dispersion Sci. Technol., 36 (2015) 61–67.
[19] L. Mouni, L. Belkhiri, J.C. Bollinger, A. Bouzaza, A. Assadi, A. Tirri, F. Dahmoune, K. Madani, H. Remini, Removal of methylene blue from aqueous solutions by adsorption on kaolin: kinetic and equilibrium studies, Appl. Clay Sci., 153 (2018) 38–45.
[20] J.M. Li, X.G. Meng, C.W. Hu, J. Du, Adsorption of phenol, p-chlorophenol and p-nitrophenol onto functional chitosan, Bioresour. Technol., 100 (2009) 1168–1173.
[21] V. Fierro, V. Torné-Fernández, D. Montané, A. Celzard, Adsorption of phenol onto activated carbons having different textural and surface properties, Microporous Mesoporous Mater., 111 (2008) 276–284.
[22] N. Tancredi, N. Medero, F. Möller, J. Píriz, C. Plada, T. Cordero, Phenol adsorption onto powdered and granular activated carbon, prepared from Eucalyptus wood, J. Colloid Interface Sci.,279 (2004) 357–363.
[23] N. Roostaei, F.H. Tezel, Removal of phenol from aqueous solutions by adsorption, J. Environ. Manage., 70 (2004) 157–164.
[24] S. Bekkouche, M. Bouhelassa, N. Hadj Salah, F.Z. Meghlaoui, Study of adsorption of phenol on titanium oxide (TiO_2), Desalination, 166 (2004) 355–362.
[25] A. Alshameri, H. He, J. Zhu, Y. Xi, R. Zhu, L. Ma, Q. Tao, Adsorption of ammonium by different natural clay minerals: characterization, kinetics and adsorption isotherms, Appl. Clay Sci., 159 (2018) 83–93. doi:10.1016/j.clay.2017.11.007.
[26] K. Srinivasarao, S.M. Prabhu, W. Luo, K. Sasaki, Enhanced adsorption of perchlorate by gemini surfactant-modified montmorillonite: synthesis, characterization and their adsorption mechanism, Appl. Clay Sci., 163 (2018) 46–55.
[27] S. Mukherjee, N.K. Gupta, S.P. Roy, S. Dash, A. Kumar, Y.R. Bamankar, T.V.V. Rao, N. Kumar, Y. Naik, Preparation of palladium impregnated alumina adsorbents: thermal and neutron activation analysis, Thermochim. Acta., 625 (2016) 56–64.
[28] P.C.C. Faria, J.J.M. Órfão, M.F.R. Pereira, Adsorption of anionic and cationic dyes on activated carbons with different surface chemistries, Water Res., 38 (2004) 2043–2052.
[29] Y.S. Al-Degs, M.I. El-Barghouthi, A.H. El-Sheikh, G.M. Walker, Effect of solution pH, ionic strength, and temperature on adsorption behavior of reactive dyes on activated carbon, Dye. Pigm., 77 (2008) 16–23.
[30] W. Bouguerraa, A. Mnifa, B. Hamrounia, M. Dhahbib, Boron removal by adsorption onto activated alumina and by reverse osmosis, Desalination., 223 (2008) 31–37.
[31] E. Worch, Adsorption Technology in Water Treatment: Fundamentals, Processes, and Modeling, 2012.
[32] R.N. Coimbra, V. Calisto, C.I.A. Ferreira, V.I. Esteves, M. Otero, Removal of pharmaceuticals from municipal wastewater by adsorption onto pyrolyzed pulp mill sludge, Arab. J. Chem., (2015). doi:10.1016/j.arabjc.2015.12.001.
[33] G. Blanchard, M. Maunaye, G. Martin, Removal of heavy metals from waters by means of natural zeolites, Water Res., 18 (1984) 1501–1507.
[34] S. Lagergren, About the Theory of So-Called Adsorption of Soluble Substances, 1898.
[35] I.S. McLintock, The Elovich equation in chemisorption kinetics, Nature, 216 (1967) 1204–1205.

[36] P. Senthil Kumar, S. Ramalingam, R.V. Abhinaya, S.D. Kirupha, A. Murugesan, S. Sivanesan, Adsorption of metal ions onto the chemically modified agricultural waste, Clean - Soil, Air, Water., 40 (2012) 188–197.
[37] P. Senthilkumar, S. Ramalingam, R.V. Abhinaya, S.D. Kirupha, T. Vidhyadevi, S. Sivanesan, Adsorption equilibrium, thermodynamics, kinetics, mechanism and process design of zinc(II) ions onto cashew nut shell, Canadian J. Chem. Eng., 90 (2012) 973–982.
[38] W.J. Weber, J.C. Morris, Kinetics of adsorption on carbon from solution, J. Sanit. Eng. Div., 89 (1963) 31–60.
[39] H.N. Tran, S.J. You, A. Hosseini-Bandegharaei, H.P. Chao, Mistakes and inconsistencies regarding adsorption of contaminants from aqueous solutions: a critical review, Water Res., 120 (2017) 88–116.
[40] M. Belhachemi, F. Addoun, Adsorption of congo red onto activated carbons having different surface properties: studies of kinetics and adsorption equilibrium, Desal. Wat. Treat., 37 (2012) 122–129.
[41] G.E. Boyd, A.W. Adamson, L.S. Myers Jr, The exchange adsorption of ions from aqueous solutions by organic zeolites. II. Kinetics1, J. Am. Chem. Soc., 69 (1947) 2836–2848.
[42] H.M.F. Freundlich, Über Die Absorption in Lösungen, Z. Phys. Chem., 57 (1906) 385–470.
[43] I. Langmuir, The adsorption of gases on plane surfaces of glass, mica and platinum, J. Am. Chem. Soc., 40 (1918) 1361–1403.
[44] V. Temkin, M.J., Pyzhev, Recent modifications to Langmuir isotherms, Acta Physiochim. URSS., 12 (1940) 217–222.
[45] L.V. Dubinin, M.M., Radushkevich, Equation of the characteristic curve of activated charcoal, Proc. Acad. Sci. Phys. Chem. Sec. USSR., 55 (1947) 331–333.
[46] O. Redlich, D.L. Peterson, A useful adsorption isotherm, J. Phys. Chem., 63 (1959) 1024–1024.
[47] C.C. Leng, N.G. Pinto, Effects of surface properties of activated carbons on adsorption behavior of selected aromatics, Carbon, 35 (1997) 1375–1385.
[48] S.M. Safwat, M. Medhat, H. Abdel-Halim, Adsorption of phenol onto aluminium oxide and zinc oxide: a comparative study with titanium dioxide, Sep. Sci. Technol., (2018) 1–13. doi.org/10.1080/01496395.2018.1549572.
[49] R. Dyanati, Z. Yousefi, J. Yazdani Cherati, D. Balarak, Investigating phenol absorption from aqueous solution by dried azolla, J. Maz. Univ. Med. Sci., 22 (2013) 13–20.
[50] M. Ahmaruzzaman, D.K. Sharma, Adsorption of phenols from wastewater, J. Colloid Interface Sci., 287 (2005) 14–24.
[51] Y.I. Tarasevich, Porous structure and adsorption properties of natural porous coal, Colloids Surf., A, 176 (2001) 267–272.
[52] V.K. Gupta, S. Sharma, I.S. Yadav, D. Mohan, Utilization of bagasse fly ash generated in the sugar industry for the removal and recovery of phenol and p-nitrophenol from wastewater, J. Chem. Technol. Biotechnol., 71 (1998) 180–186.